Delay Growth Model augmented with Physical and Human Capitals: Revised Version

Akio Matsumoto
Chuo University

Ferenc Szidarovszky
Corvinus University

July 2019

INSTITUTE OF ECONOMIC RESEARCH
Chuo University
Tokyo, Japan

Delay Growth Model augmented with Physical and Human Capitals: Revised Version[*]

Akio Matsumoto[†]   Ferenc Szidarovszky[‡]

Abstract

A growth model with a special production function augmented with physical capital and human capital is modified and used to explain the birth of cyclical dynamics. Crucial feature of the model is the assumption that there are a gestation delay and a maturation delay in constructing physical capital and human capital, respectively. Dynamics is described by a continuous time system of delay differential equations. Stability switching curves are analytically derived on which stability of the model is lost. Its shape is numerically verified and it is confirmed that the two-delay model can generate a wide variety of dynamics from simple dynamics to complex dynamics.

Keywords: Extended Solow model, Delayed dynamics, Two delays, Asymptotic behavior

1   Introduction

Most classical models in mathematical economics assume that instantaneous data are always available to all participants and they are able to react immediately. However, in real economies this is only an approximation of reality, since collecting data, their analysis, decision making and implementation need time. This is the reason why models including time delays became one of the major research fields recently.

This study examines dynamics of an extended Solow model (Solow, 1956) augmented with physical and human capitals incorporating time delays due to gestation time in physical capital and maturation time in human capital. It

[†]Professor, Department of Economics, Chuo University, 742-1, Higashi-Nakano, Hachioji, Tokyo, 192-0393, Japan; akiom@tamacc.chuo-u.ac.jp

[‡]Professor, Department of Mathematics, Corvinus University, Budapest, Fövám tèr 8, H-1093, Hungary, szidarka@gmail.com

will be shown that the delays could destabilize an otherwise stable model and generate persistent oscillations that might be compatible with actually observed data.

Gori et al. (2016) offer survey of related studies and consider an extended Solow model with physical and human capitals that is exactly the same as what we study. There are similarities as well as dissimilarities. Approaching the main purpose to see how the two delays affect stability of the model is different. We make two-dimensional analysis in which both delays vary continuously, whereas they adopt a repeated one-dimensional analysis in which one delay is assumed to be positive and fixed and the other delay varies. Their analysis is based on an assumption that a mixed polynomial-trigonometric equation (Eq.(22)) has finitely many roots. This assumption makes their analysis incomplete unless the assumption is justified. We can also derive the directions of the stability switches based on analytic representations of the stability switching curves. We focus mainly on the symmetric case with only limited attention to the asymmetric case while they do not look into the symmetric case. The analytical results obtained in the symmetric case could be bases for analyzing the asymmetric case. Due to these differences, we can arrive at new results. Hence our study might complement their study. Further, this paper is a continuation of the earlier studies giving a complete stability analysis with analytic representations of the stability switching curves and the directions of the stability switches. We also examine a special case which was not studied earlier.

The rest of the paper is organized as follows. Section 2 reviews a special version of the extended Solow model. Section 3 introduces delays in physical and human capitals and investigates the effects caused by two delays on dynamics. Section 4 numerically validates the analytical results obtained in the previous sections. Finally concluding remarks are given in Section 5.

2 Extended Growth Model

Before proceeding the analysis, we first review the continuous-time Solow model. Only for the sake of simplicity, a special Cobb-Douglas production function is adopted,

$$Y(t) = K(t)^\alpha \left[A(t)L(t)\right]^{1-\alpha}, \ 0 < \alpha < 1 \tag{1}$$

where t denotes time, $Y(t)$ represents output, $L(t)$ labor, $K(t)$ the physical capital stock and $A(t)$ the labor-augment technology. The physical capital accumulation is described by

$$\dot{K}(t) = sY(t) - \delta K(t) \tag{2}$$

where the dot over a variable means a time-derivative, s is the saving rate, $0 < s < 1$, and δ the depreciation rate, $\delta > 0$. Dividing the accumulation equation by effective labor $A(t)L(t)$ transforms it to a per capita form

$$\dot{k}(t) = sk(t)^\alpha - (n + g + \delta)k(t) \tag{3}$$

where

$$k(t) = \frac{K(t)}{A(t)L(t)}, \; y(t) = \frac{Y(t)}{A(t)L(t)} = k(t)^\alpha$$

and the constant growth rates of labor and technology are n and g, respectively.

A positive steady state is given as

$$k_S^* = \left(\frac{s}{n+g+\delta} \right)^{\frac{1}{1-\alpha}}.$$

At the steady state, the stock of physical capital and output are growing at the constant rate $n+g$,

$$\frac{\dot{K}(t)}{K(t)} = \frac{\dot{Y}(t)}{Y(t)} = n+g.$$

It is to be noticed that both growth rates are exogenously given and thus the growth of per capita output occurs only due to exogenous technology change.

Mankiw, Romer and Weil (1992, MRW henceforth), assumes an extended Cobb-Douglas production function to have three factors,

$$Y(t) = K(t)^\alpha H(t)^\beta \left[A(t)L(t) \right]^{1-\alpha-\beta}$$

where $1 - \alpha - \beta > 0$, $\alpha > 0$ and $\beta > 0$. H is the stock of human capital. Physical capital and human capital are formed by saving an s_k-fraction and an s_h-fraction of output with $s_k > 0$, $s_h > 0$ and $s_k + s_h < 1$. The accumulation of these per capita capital stocks is determined by

$$\dot{k}(t) = s_k k(t)^\alpha h(t)^\beta - (n+g+\delta)k(t)$$

$$\dot{h}(t) = s_h k(t)^\alpha h(t)^\beta - (n+g+\delta)h(t)$$

(4)

where $k(t)$ is already defined and $h(t)$ is the stock of human capital per capita defined by

$$h(t) = \frac{H(t)}{A(t)L(t)}.$$

A steady state is given as

$$k^* = \left(\frac{s_k^{1-\beta} s_h^\beta}{n+g+\delta} \right)^{\frac{1}{1-\alpha-\beta}},$$

$$h^* = \left(\frac{s_k^\alpha s_h^{1-\alpha}}{n+g+\delta} \right)^{\frac{1}{1-\alpha-\beta}}.$$

(5)

Nonnegative values of k^* and h^* lead the following conditions at the steady state at which $\dot{k}(t) = \dot{h}(t) = 0$,

$$s_k \left(k^* \right)^{\alpha-1} \left(h^* \right)^\beta = c,$$

$$s_h \left(k^* \right)^\alpha \left(h^* \right)^{\beta-1} = c$$

(6)

3

with $n + g + \delta = c$. It is well-known that the dynamic system (4) converges to the steady state under the assumption of diminishing returns to scale (i.e., $\alpha + \beta < 1$):

Theorem 1 *The positive stationary point (h^*, k^*) of extended Solow model (4) is locally asymptotically stable.*

3   Stability Switching Curves

In á la Solow models, dynamics has two phases. In the first phase, the economy starting at any initial state sooner or later converges to the steady state. On a transition path to the steady state, per capita growth rate is non-zero and becomes zero when it arrives at the steady state. In the second phase the long-run dynamics is conducted by the population growth and the technological development. We focus on the evolution of the economy in the first phase. To this end, we assume the following to get rid of the exogenous shocks.

Assumption 1: $n = g = 0$.

We now turn attention to a delay version of MRW's stock accumulation system of physical and human capitals

$$\dot{k}(t) = s_k k(t - \tau_k)^\alpha h(t - \tau_h)^\beta - \delta k(t - \tau_k)$$

$$\dot{h}(t) = s_h k(t - \tau_k)^\alpha h(t - \tau_h)^\beta - \delta h(t - \tau_h)$$

(7)

with $\tau_k \geq 0$ and $\tau_h \geq 0$. Using the relations in (6) yields the linearized delay system,

$$\dot{k}(t) = \delta(\alpha - 1)k(t - \tau_k) + \beta\delta\frac{s_k}{s_h}h(t - \tau_k),$$

$$\dot{h}(t) = \alpha\delta\frac{s_h}{s_k}k(t - \tau_h) + \delta(\beta - 1)h(t - \tau_h).$$

(8)

The corresponding characteristic equation is

$$P_0(\lambda) + P_1(\lambda)e^{-\lambda\tau_k} + P_2(\lambda)e^{-\lambda\tau_h} + P_3(\lambda)e^{-\lambda(\tau_k+\tau_h)} = 0 \qquad (9)$$

where

$$P_0(\lambda) = \lambda^2,$$

$$P_1(\lambda) = \delta(1 - \alpha)\lambda,$$

$$P_2(\lambda) = \delta(1 - \beta)\lambda,$$

$$P_3(\lambda) = \delta^2 \left(1 - \alpha - \beta\right).$$

4

As a benchmark, we start with the no-delay case in which $\tau_k = \tau_h = 0$. The characteristic equation (9) is now written as

$$\lambda^2 + \delta\left[(1-\alpha) + (1-\beta)\right]\lambda + \delta^2\left(1-\alpha-\beta\right) = 0. \tag{10}$$

Since the linear coefficient and the constant term are both positive, the roots are either real negative or complex with negative real parts implying asymptotical stability. Since one-delay models are discussed earlier in the literature in detail, we concentrate only on the two-delay symmetric case when $\alpha = \beta$ with $\alpha < 1/2$.

Assumption 2: $\alpha = \beta$.

We now suppose that $\tau_k > 0$ and $\tau_h > 0$ and find all pure complex roots of the characteristic equation of (9). We can also assume that $\lambda = i\omega$ with $\omega > 0$. Substituting this solution into (9) presents the following form of the characteristic equation,

$$P_0(i\omega) + P_1(i\omega)e^{-i\omega\tau_k} + P_2(i\omega)e^{-i\omega\tau_h} + P_3(i\omega)e^{-i\omega(\tau_k+\tau_h)} = 0 \tag{11}$$

where

$$P_0(i\omega) = -\omega^2,$$

$$P_1(i\omega) = i\delta(1-\alpha)\omega,$$

$$P_2(i\omega) = i\delta(1-\alpha)\omega,$$

$$P_3(i\omega) = \delta^2\left(1-2\alpha\right).$$

Applying the method developed by Matsumoto and Szidarovszky (2018) based on Lin and Wang (2012), we can derive the set of points (τ_k, τ_h) for which the delay dynamic system (7) might lose stability. Equation (11) can be written as

$$P_0(i\omega) + P_1(i\omega)e^{-i\omega\tau_k} + \left(P_2(i\omega) + P_3(i\omega)e^{-i\omega\tau_k}\right)e^{-i\omega\tau_h} = 0. \tag{12}$$

Since $\left|e^{-\lambda\omega\tau_h}\right| = 1$, equation (12) has solution if and only if

$$\left|P_0(i\omega) + P_1(i\omega)e^{-i\omega\tau_k}\right| = \left|P_2(i\omega) + P_3(i\omega)e^{-i\omega\tau_k}\right|$$

or equivalently,

$$\left(P_0(i\omega) + P_1(i\omega)e^{-i\omega\tau_k}\right)\left(\bar{P}_0(i\omega) + \bar{P}_1(i\omega)e^{i\omega\tau_k}\right)$$
$$= \left(P_2(i\omega) + P_3(i\omega)e^{-i\omega\tau_k}\right)\left(\bar{P}_2(i\omega) + \bar{P}_3(i\omega)e^{i\omega\tau_k}\right)$$

where over-bar indicates complex conjugate. After some calculations, the last equation can be rewritten as

$$|P_0|^2 + |P_1|^2 - |P_2|^2 - |P_3|^2 = 2A_k(\omega)\cos\omega\tau_k - 2B_k(\omega)\sin\omega\tau_k \tag{13}$$

where the argument of P_i is omitted for the sake of notational simplicity and

$$A_k(\omega) = \mathrm{Re}\left(P_2\bar{P}_3 - P_0\bar{P}_1\right) \text{ and } B_k(\omega) = \mathrm{Im}\left(P_2\bar{P}_3 - P_0\bar{P}_1\right).$$

Using $P_i(i\omega)$ for $i = 0, 1, 2, 3$, we can obtain

$$P_2\bar{P}_3 - P_0\bar{P}_1 = i\delta\omega(1 - \alpha)\left[\delta^2(1 - 2\alpha) - \omega^2\right].$$

Hence

$$A_k(\omega) = 0$$

and

$$B_k(\omega) = \delta\omega\left[\delta^2(1 - \alpha)(1 - 2\alpha) - \omega^2(1 - \alpha)\right].$$

The sign of $B_k(\omega)$ is indeterminate. The corresponding values of τ_h as functions of τ_k can be obtained from equation (12) as

$$e^{-i\omega\tau_h} = -\frac{P_0(i\omega) + P_1(i\omega)e^{-i\omega\tau_k}}{P_2(i\omega) + P_3(i\omega)e^{-i\omega\tau_k}} \tag{14}$$

where the absolute value of the right hand side has to be the unity.

An explicit form of τ_h satisfying equation (14) is derived as follows. Due to the Euler's formula, (14) can be rewritten as

$$\cos\omega\tau_h - i\sin\omega\tau_h = \frac{\boldsymbol{a} - i\boldsymbol{b}}{\boldsymbol{c} + i\boldsymbol{d}} \tag{15}$$

where

$$\boldsymbol{a} = \omega^2 - \delta\omega(1 - \alpha)\sin\omega\tau_k, \ \boldsymbol{b} = \delta\omega(1 - \alpha)\cos\omega\tau_k$$

and

$$\boldsymbol{c} = \delta^2(1 - 2\alpha)\cos\omega\tau_k, \ \boldsymbol{d} = \delta\omega(1 - \alpha) - \delta^2(1 - 2\alpha)\sin\omega\tau_k.$$

The right hand side is next developed. Multiplying the denominator and the numerator of (15) by the conjugate of the denominator, the denominator, after arranging the terms, becomes

$$D = \delta^2\left[\delta^2(1 - 2\alpha)^2 + \omega^2(1 - \alpha)^2 - 2\delta\omega(1 - \alpha)(1 - 2\alpha)\sin\omega\tau_k\right]$$

which is always positive as $D = \boldsymbol{c}^2 + \boldsymbol{d}^2$. The new numerator can be denoted by $M + iN$ where the real part is

$$M = -\left(\delta\omega\right)^2\alpha^2\cos\omega\tau_k$$

and the imaginary part is

$$N = -\delta\omega\left\{\delta^2(1 - \alpha)(1 - 2\alpha) + \omega^2(1 - \alpha) - \delta\omega\left[2(1 - 2\alpha) + \alpha^2\right]\sin\omega\tau_k\right\}.$$

Comparing the left hand side of (15) with $M/D + iN/D$ presents

$$\cos\omega\tau_h = \frac{M}{D} \text{ and } \sin\omega\tau_h = -\frac{N}{D}. \tag{16}$$

Denoting the left hand side of equation (13) by $f(\omega)$, we confirm solutions of (13), that is, $f(\omega) = -2B_k(\omega)\sin\omega\tau_k$. Dividing the remaining of this section into two, we examine the case of $B_k(\omega) = 0$ in the first part and then proceed to the case of $B_k(\omega) \neq 0$ in the second.

3.1 $B_k(\omega) = 0$

Let ω_k be the positive solution of $B_k(\omega) = 0$,

$$\omega_k = \delta\sqrt{1 - 2\alpha} > 0.$$

Substituting $P_i(i\omega)$ for $i = 0, 1, 2, 3$ into $f(\omega)$ gives

$$f(\omega) = \omega^4 - \delta^4(1 - 2\alpha)^2.$$

Solving $f(\omega) = 0$ for ω^2 presents the positive solution,

$$\omega_+^2 = \delta^2(1 - 2\alpha) > 0.$$

The critical value and the positive solution become identical,

$$\omega_k^2 = \omega_+^2 = \delta^2(1 - 2\alpha) > 0.$$

In the symmetric case, $f_k(\omega) = 0$ for $\omega = \omega_k$ at which, therefore, the value of τ_k is arbitrary and the corresponding values of τ_h can be obtained from (16).

The graphs of M/D and $-N/D$ are illustrated for $\tau_k \in \left[0, 20\sqrt{3}\pi/\omega\right]$ with the parameter values of $\alpha = 1/3$ and $\delta = 1/10$ in Figure 1.[1] The red M/D curve intersects the horizontal axis twice at which $\cos\omega\tau_k = 0$, implying that $\omega\tau_k = \pi/2$ at point B and $\omega\tau_k = 3\pi/2$ at point D,

$$\tau_k^B = \frac{\pi}{2\omega_k} \simeq 24.72 \text{ and } \tau_k^D = \frac{3\pi}{2\omega_k} \simeq 81.62.$$

It is also seen that the blue $-N/D$ curve intersects the horizontal axis twice at which $N = 0$ or

$$\sin\omega\tau_k \quad = \frac{\delta^2(1 - \alpha)(1 - 2\alpha) + \omega_k^2(1 - \alpha)}{\delta\omega_k\left[2(1 - 2\alpha) + \alpha^2\right]}$$

$$= \frac{2(1 - \alpha)\sqrt{1 - 2\alpha}}{(\alpha - 2)^2 - 2} < 1 \text{ for } 0 < \alpha < \frac{1}{2}.$$

Since $\sin\omega\tau_k$ takes the maximum value at $\omega\tau_k = \pi/2$, $\sin\omega\tau_k^A = 4\sqrt{3}/7$ and $\cos\omega\tau_k^A > 0$ at point A and $\sin\omega\tau_k^B = 4\sqrt{3}/7$ and $\cos\omega\tau_k^B < 0$ at point B, implying that

$$\tau_k^A = \frac{1}{\omega_k}\sin^{-1}\left(\frac{4\sqrt{3}}{7}\right) \simeq 24.72 \text{ and } \tau_k^C = \frac{1}{\omega_k}\left[\pi - \sin^{-1}\left(\frac{4\sqrt{3}}{7}\right)\right] \simeq 29.69.$$

---

[1]MRW presumes that α is about one third and β is between one third and one half.
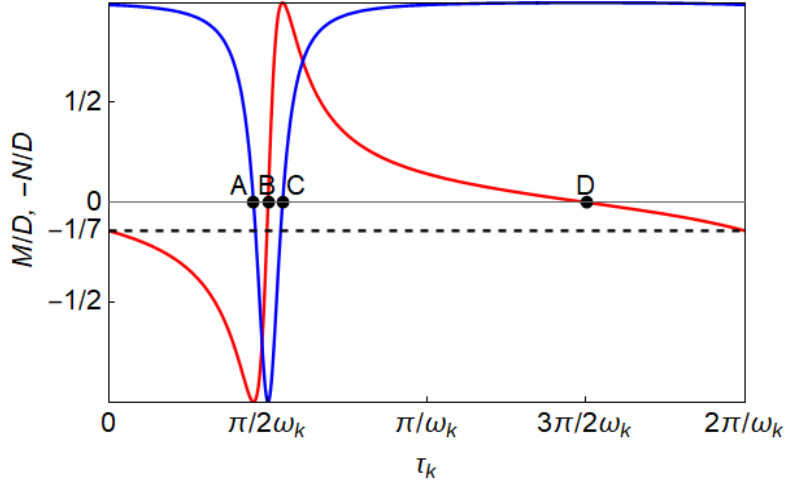
Figure 1. Graphs of M/D (red) and $-N/D$ (blue)

The interval $[0, 2\pi/\omega_k]$ is divided into five subintervals by those points. It is observed that $\cos\omega\tau_h < 0$ and $\sin\omega\tau_h > 0$ for $\tau_k \in (0, \tau_k^A)$. Hence solving $\cos\omega_k\tau_h = M/D$ and $\sin\omega_k\tau_h = -N/D$ for τ_h yields

$$\tau_h^c(\tau_k) = \frac{1}{\omega_k}\cos^{-1}\left(\frac{M}{D}\right) \text{ and } \tau_h^s(\tau_k) = \frac{1}{\omega_k}\left[\pi - \sin^{-1}\left(-\frac{N}{D}\right)\right]. \qquad (17)$$

where the superscripts c and s stand for cos and sin, respectively. In the same way, $\cos\omega_k\tau_h < 0$ and $\sin\omega_k\tau_h < 0$ for $\tau_h \in (\tau_k^A, \tau_k^B)$ that present

$$\tau_h^c(\tau_k) = \frac{1}{\omega_k}\left[2\pi - \cos^{-1}\left(\frac{M}{D}\right)\right] \text{ and } \tau_h^s(\tau_k) = \frac{1}{\omega_k}\left[\pi - \sin^{-1}\left(-\frac{N}{D}\right)\right]. \qquad (18)$$

For $\tau_k \in (\tau_k^B, \tau_k^C)$, $\cos\omega_k\tau_k > 0$ and $\sin\omega_k\tau_k < 0$ gives

$$\tau_h^c(\tau_k) = \frac{1}{\omega_k}\left[2\pi - \cos^{-1}\left(\frac{M}{D}\right)\right] \text{ and } \tau_h^s(\tau_k) = \frac{1}{\omega_k}\left[2\pi + \sin^{-1}\left(-\frac{N}{D}\right)\right]. \qquad (19)$$

For $\tau_k \in (\tau_k^C, \tau_k^D)$, $\cos\omega_h\tau_k > 0$ and $\sin\omega_h\tau_k > 0$ generating

$$\tau_h^c(\tau_k) = \frac{1}{\omega_k}\cos^{-1}\left(\frac{M}{D}\right) \text{ and } \tau_h^s(\tau_k) = \frac{1}{\omega_k}\sin^{-1}\left(-\frac{N}{D}\right). \qquad (20)$$

Finally, we have $\cos\omega_h\tau_k < 0$ and $\sin\omega_h\tau_k > 0$ for $\tau_k \in (\tau_k^D, 2\pi/\omega_k)$ in which case the signs of the trigonometric functions are the same as in the first case. Hence, from (17)

$$\tau_h^c(\tau_k) = \frac{1}{\omega_k}\cos^{-1}\left(\frac{M}{D}\right) \text{ and } \tau_h^s(\tau_k) = \frac{1}{\omega_k}\left[\pi - \sin^{-1}\left(-\frac{N}{D}\right)\right]. \qquad (21)$$

Since $\tau_h^s(\tau_k) = \tau_h^c(\tau_k)$ holds for any $\tau_k \in [0, 2\pi/\omega]$, the solution can be denoted by $\tau_h(\tau_k)$.

8

The locus of $(\tau_k, \tau_h(\tau_k))$ for $\tau_k \in [0, 2\pi/\omega]$ constructs the stability switching curve that is illustrated by two black-red curves in Figure 2. More precisely, the upper convex-shaped curve consists of three segments, each of which is described by the black segment (17), the red segment, (18) and the black segment, (19) whereas the lower concave-shaped curve is described by the red segment (20) and the black segment, (21). The results obtained are summarized as follows:

Lemma 1 *If $B_k(\omega) = 0$ in the symmetric case, then the stability switching curve is described by the locus of $(\tau_k, \tau_h(\tau_k))$ where*

$$\tau_h(\tau_k) = \frac{1}{\omega_k} \cos^{-1}\left(\frac{M}{D}\right) \ \text{ for } \tau_k \in (0, \tau_k^A) \cup (\tau_k^C, \tau_k^D) \cup (\tau_k^D, 2\pi/\omega_k)$$

and

$$\tau_h(\tau_k) = \frac{1}{\omega_k}\left[2\pi - \cos^{-1}\left(\frac{M}{D}\right)\right] \ \text{ for for } \tau_k \in (\tau_k^A, \tau_k^B) \cup (\tau_k^B, \tau_k^C).$$

Two issues should be noticed. First, in the symmetric case and $B_k(\omega) = 0$, Lemma 4 of Gori et a. (2016) is a special case of this Lemma 1. In particular, their critical value of delay, $\tau_{2,j}$ of their equation (17) with $j = 0$ is equal to

$$\tau_h(0) = \frac{1}{\omega_k} \cos^{-1}\left(-\frac{1}{7}\right) \simeq 29.6898.$$

This value corresponds to the τ_h-value of the intercept of the vertical axis with the convex-shaped black curve in Figure 2. Second, if $B_k(\omega) = 0$ and $\alpha \neq \beta$, then no stability switching occurs, so the positive steady state is locally asymptotically stable for all positive values of τ_k and τ_h.
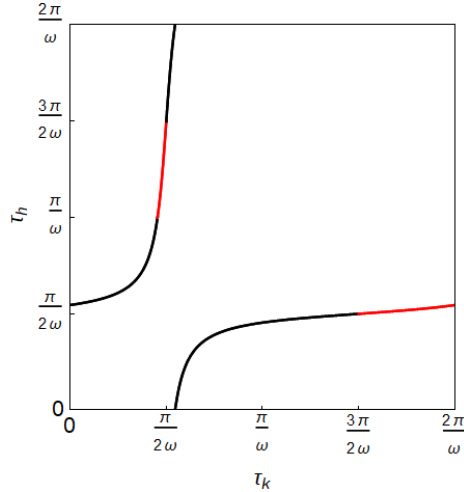
Figure 2. Stability switching curve with $B_k(\omega) = 0$

3.2 $|B_k(\omega)|^2 > 0$

We have already shown that $A_k(\omega) = 0$ for any $\omega \geq 0$ and $B_k(\omega) \neq 0$ for $\omega \neq \omega_k$. Then there exists $\varphi_k(\omega)$ such that

$$\varphi_k(\omega) = \arg\left[P_2\bar{P}_3 - P_0\bar{P}_1\right] = \begin{cases} \dfrac{\pi}{2} \text{ if } B_k(\omega) > 0 \text{ or } \omega < \omega_k, \\[2mm] \dfrac{3\pi}{2} \text{ if } B_k(\omega) < 0 \text{ or } \omega > \omega_k, \end{cases}$$

implying that

$$\sin\left[\varphi_k(\omega)\right] = \frac{B_k(\omega)}{\sqrt{B_k(\omega)^2}} = \pm 1 \text{ and } \cos\left[\varphi_k(\omega)\right] = \frac{A_k(\omega)}{\sqrt{B_k(\omega)^2}} = 0.$$

Using these relations and the addition theorem, equation (13) can be reduced to

$$|P_0|^2 + |P_1|^2 - |P_2|^2 - |P_3|^2 = 2\sqrt{B_k(\omega)^2}\cos\left[\varphi_k(\omega) + \omega\tau_k\right] \tag{22}$$

that can be rewritten as

$$\frac{|P_0|^2 + |P_1|^2 - |P_2|^2 - |P_3|^2}{2\sqrt{B_k(\omega)^2}} = \cos\left[\varphi_k(\omega) + \omega\tau_k\right] \leq 1.$$

Hence a sufficient and necessary condition for the existence of $\tau_k \geq 0$ satisfying the above equation is

$$\left| |P_0|^2 + |P_1|^2 - |P_2|^2 - |P_3|^2 \right| \leq 2\sqrt{B_k(\omega)^2}$$

or

$$F(\omega) = \left[|P_0|^2 + |P_1|^2 - |P_2|^2 - |P_3|^2\right]^2 - 4B_k(\omega)^2 \leq 0.$$

With the notation of $x = \omega^2$, the right hand side of $F(\omega)$ is reduced to the following form,

$$F(x) = x^4 + a_3 x^3 + a_2 x^2 + a_1 x + a_0 \tag{23}$$

where the coefficients are defined as

$$a_3 = -4\delta^2(1-\alpha)^2,$$

$$a_2 = 2\delta^4(1-2\alpha)\left[4(1-\alpha)^2 + (1-2\alpha)\right],$$

$$a_1 = -4\delta^6(1-2\alpha)^2(1-\alpha)^2,$$

$$a_0 = \delta^8(1-2\alpha)^4.$$

The factored form of (23) becomes

$$F(x) = \left(x - \delta^2\right)\left(x - \delta^2(1-2\alpha)^2\right)\eta(x) \tag{24}$$

where
$$\eta(x) = x^2 - 2\delta^2(1 - 2\alpha)x - \delta^4(1 - 2\alpha)^2.$$

Solving $F(x) = 0$ yields four real solutions,

$$x_1 = \delta^2 > 0,$$

$$x_2 = \delta^2(1 - 2\alpha)^2 > 0,$$

$$x_3 = x_4 = \delta^2(1 - 2\alpha),$$

implying that $x_2 < x_3 = x_4 < x_1$, so $\omega_2 < \omega_3 = \omega_4 < \omega_1$. It is also clear that $F(\omega) \leq 0$ if $\omega_2 \leq \omega \leq \omega_1$.

Let us define $\psi_k(\omega)$ by

$$|P_0|^2 + |P_1|^2 - |P_2|^2 - |P_3|^2 = 2\sqrt{B_k(\omega)^2}\cos[\psi_k(\omega)] \tag{25}$$

or

$$\psi_k(\omega) = \cos^{-1}\left[\frac{|P_0|^2 + |P_1|^2 - |P_2|^2 - |P_3|^2}{2\sqrt{B_k(\omega)^2}}\right].$$

Comparing the right hand side of (22) with that of (25) presents

$$\tau_{k,m}^{\pm}(\omega) = \frac{1}{\omega}\left[\pm\psi_k(\omega) - \varphi_k(\omega) + 2m\pi\right]. \tag{26}$$

Returning to (11), we can see that it can be alternatively written as

$$P_0 + P_2 e^{-i\omega\tau_h} + \left(P_1 + P_3 e^{-i\omega\tau_h}\right)e^{-i\omega\tau_k} = 0. \tag{27}$$

The similarity of (27) to (12) is clear. Hence, in the similar way to deriving $\tau_{k,m}^{\pm}(\omega)$, we can define the critical values of τ_h as

$$\tau_{h,n}^{\pm}(\omega) = \frac{1}{\omega}\left[\pm\psi_h(\omega) - \varphi_h(\omega) + 2n\pi\right]. \tag{28}$$

It is easy to show that

$$\begin{aligned}
A_h(\omega) &= \operatorname{Re}\left[P_1\bar{P}_3 - P_0\bar{P}_2\right] = 0,\\
B_h(\omega) &= \operatorname{Im}\left[P_1\bar{P}_3 - P_0\bar{P}_2\right] = \delta\omega(1 - \alpha)\left[\delta^2(1 - 2\alpha) - \omega^2\right],
\end{aligned}$$

$$\psi_h(\omega) = \cos^{-1}\left[\frac{|P_0|^2 - |P_1|^2 + |P_2|^2 - |P_3|^2}{2\sqrt{B_h(\omega)^2}}\right]$$

and

$$\varphi_h(\omega) = \arg\left[P_1\bar{P}_3 - P_0\bar{P}_2\right] = \begin{cases} \dfrac{\pi}{2} & \text{if } B_h(\omega) > 0 \text{ or } \omega < \omega_h,\\[2ex] \dfrac{3\pi}{2} & \text{if } B_h(\omega) < 0 \text{ or } \omega > \omega_h \end{cases}$$

11

with ω_h being the positive solution of $B_h(\omega) = 0$,

$$\omega_h = \delta\sqrt{1 - 2\alpha}.$$

In case of $B_h(\omega) = 0$, we solve (27) to have

$$e^{-i\omega\tau_k} = -\frac{P_0 + P_2 e^{-i\omega\tau_h}}{P_1 + P_3 e^{-i\omega\tau_h}}. \tag{29}$$

Two remarks should be addressed. First, as in the same way as to derive $\tau_h(\tau_k)$ from equation (14), we can obtain $\tau_k(\tau_h)$ and the stability switching curve $(\tau_k(\tau_h), \tau_h)$ from equation (29). And second, noticing that (14) and (29) are different equations derived from the same equation (12), we can see that the stability switching curve $(\tau_k(\tau_h), \tau_h)$ is identical with the stability switching curve $(\tau_h(\tau_k), \tau_k)$. In case of $B_h(\omega) \neq 0$, we can define critical values of τ_h. To define $\psi_h(\omega)$, we need a condition similar to $F(\omega) \leq 0$, that is,

$$G(\omega) = \left[|P_0|^2 - |P_1|^2 + |P_2|^2 - |P_3|^2\right]^2 - 4B_h(\omega)^2 \leq 0.$$

It can be shown that inequlities $F(\omega) \leq 0$ and $G(\omega) \leq 0$ define the same domain for ω.

In the symmetric case,

$$\omega_k = \omega_h = \omega_3 = \omega_4 = \delta\sqrt{1 - 2\alpha}.$$

Hence, for $\omega < \omega_k = \omega_h$, $\varphi_k(\omega) = \varphi_h(\omega) = \pi/2$.[2] The blue and red curves in Figure 3 are the stability switching curves and described, respectively, by

$$\left(\tau_{k,0}^+(\omega), \tau_{h,1}^-(\omega)\right) \text{ for } \omega \in [\omega_2, \omega_3] \tag{30}$$

and

$$\left(\tau_{k,0}^-(\omega), \tau_{h,1}^+(\omega)\right) \text{ for } \omega \in [\omega_2, \omega_3]. \tag{31}$$

In the same way, for $\omega > \omega_k = \omega_h$, $\varphi_k(\omega) = \varphi_h(\omega) = 3\pi/2$. The green and orange curves are also the stability switching curves and described, respectively, by

$$\left(\tau_{k,1}^+(\omega), \tau_{h,1}^-(\omega)\right) \text{ for } \omega \in [\omega_4, \omega_1] \tag{32}$$

and

$$\left(\tau_{k,1}^-(\omega), \tau_{h,1}^+(\omega)\right) \text{ for } \omega \in [\omega_4, \omega_1]. \tag{33}$$

As can be seen in Figure 3, these loci construct egg-shaped closed curves. The blue segment of the closed curve in the bottom-left is obtained for $m = 1$ and

---

[2] As before we take $\alpha = \beta = 1/3$ and $\delta = 1/10$ under which $\omega_1 = 1/10$, $\omega_2 = 1/30 \simeq 0.0333$ and for $j = 3, 4, k, h$,

$$\omega_j = \frac{1}{10\sqrt{3}} \simeq 0.0577.$$

$n = 0$, the red one is for $m = 0$ and $n = 1$, the green and orange ones are for $m = n = 1$. Since equations (26) and (28) indicate that m is a horizontal shift parameter and n is a vertical shift parameter, increasing the value of m shifts the closed curve rightward, increasing the value of n shifts the closed curve upward, increasing both values makes the shift in the diagonal direction with some distortion. Notice that there are infinitely many closed curves since m and n can take infinitely many values. The result obtained so far is summarized as follows:

Lemma 2 *From (26) and (28) in the symmetric case the following pairs of delays,*

$$\left\{ \left(\tau_{k,m}^{\pm}(\omega), \tau_{h,n}^{\mp}(\omega) \right) \mid \omega \in \Omega \right\} \ \text{for } m, n = 0, 1, 2, ...$$

construct the set of all stability switching curves on the (τ_k, τ_h) plane for equations (7) when $B_k(\omega) \neq 0$.
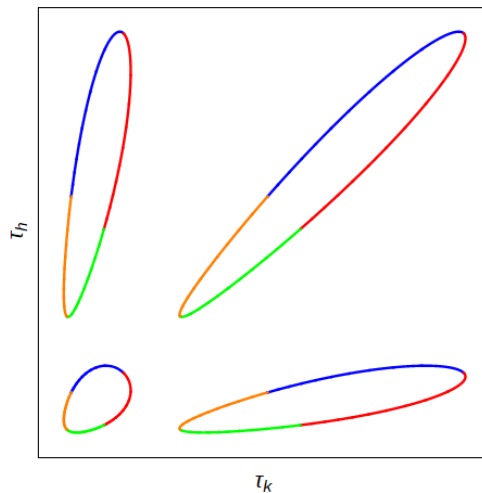
Figure 3. Stability switching curves for $m, n = 0, 1, 2$

The stability switching curve is obtained by placing Figure 2 over the lower-left part of Figure 3 that is illustrated in Figure 4. It has already been confirmed that the stationary point without delays is locally asymptotically stable. Since the stability region must includes the origin (i.e., $\tau_k = \tau_h = 0$), it might be the region surrounded by the two black, orange and green curves. If a pair of the delay is selected from this region, then the steady state of the delay system (7) is locally asymptotically stable as the real parts of the characteristic roots are negative for τ_k and τ_h. If a pair of (τ_k, τ_h) crosses one of the boundary segments, then the real part of a characteristic root becomes positive and thus the stationary state loses stability. Applying the stability switching index obtained in the Appendix, we can verify the stability switching direction along these colored critical curves. We examine the pair on the green and orange curves, the lower part of the egg-shaped ellipse. Since those curves are described by

13

(32) and (33), substituting $\tau_{k,1}^+(\omega)$ and $\tau_{k,1}^-(\omega)$ into τ_k of (A-7) and numerically calculating the corresponding indices yields the following,

$$Q[\omega, \omega\tau_{k,1}^+(\omega)] = Q_G(\omega) < 0 \text{ for } \omega \in (\omega_4, \omega_1) \text{ for the green curve,}$$

$$Q[\omega, \omega\tau_{k,1}^-(\omega)] = Q_O(\omega) > 0 \text{ for } \omega \in (\omega_4, \omega_1) \text{ for the orange curve}$$

where the subscripts G and O stand for "Green" and "Orange." According to Theorem 3, in crossing either the orange curve or the green curve from inside to outside of the closed curve at least one pair of eigenvalues changes its real part from positive to negative. On the other hand, since the index Q becomes zero along the black convex- and concave-shaped curves, neither direction of stability switch nor Hopf bifurcation can be proved.[3] However, numerical simulations indicate the loss of stability and the birth of a limit cycle as will be seen later when the pair of the delays crosses the black curve.
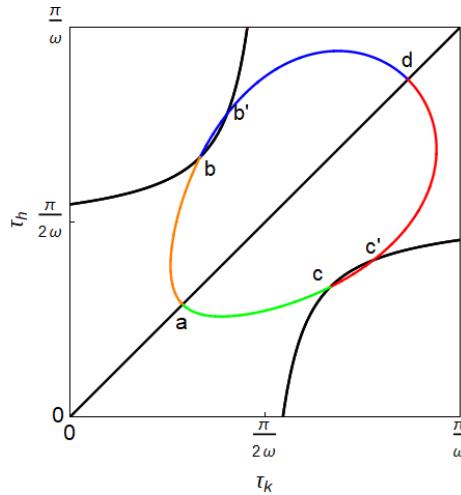
Figure 4. Stability switching curve for

One more result is added. There are two small lens-shaped regions in the lower-right and upper-left parts of Figure 4: one surrounded by the red and the concave black curves between points c and c' and the other is by the blue and the convex black curves between points b and b'. It will be numerically checked in the next section that the steady state is locally asymptotically stable in these regions. Since the steady state is unstable in the adjacent regions, the stability regain occurs when the pair of the delays crosses the boundary of these lens-shaped regions. The lower-right lens-shaped region is enlarged in Figure 5. We will return to the dotted line later. We summarize this as follows.

Theorem 2 *In the symmetric case, the steady state is locally asymptotically stable in the following two regions, one is between the two curves,*

$$\tau_h(\tau_k) \text{ for } \tau_k \in (0, \tau_k^A) \text{ and } \left(\tau_{k,0}^+(\omega), \tau_{h,1}^-(\omega)\right) \text{ for } \omega \in (\omega_2, \omega_3)$$

---

[3]The second derivative of λ can be used and check the sign change of its real part. However it would lead to very complicated expressions.

14

and the other is between the two curves

$$\tau_h(\tau_k) \ \text{for} \ \tau_k \in (\tau_k^C, \tau_k^D) \ \text{and} \ \left(\tau_{k,0}^-(\omega), \tau_{h,1}^+(\omega)\right) \ \text{for} \ \omega \in (\omega_2, \omega_3)$$
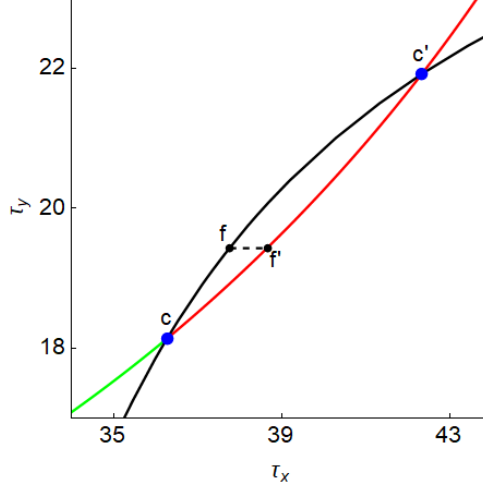
Figure 5 The lenze-shaped stability region

3.3 Two Delay Model: Asymmetric Case

In this section, the notations of the Appendix are used. We now turn attention briefly to the asymmetric case in which $\alpha = 3/10$ and $\beta = 1/3$, leading to $\alpha < \beta$ under which no possibility of $B_k(0) = 0$. The corresponding stability switching curves obtained under $|B_k(\omega)|^2 > 0$ are distorted due the parameter asymmetry and seen in Figure 6 where R_G, R_O and R_B denote the R-regions of the green, orange and blue curve, respectively. L_G, L_O and L_B denote the L-regions. The blue, green and orange curves are described by (30), (31) and (32) with the new parameter value of α and β and the same values of the other parameters. The stability switching indices can be obtained similarly to the symmetric case, and along these curves are

$$Q[\omega, \omega\tau_{k,0}^+(\omega)] = Q_B(\omega) < 0 \text{ for } \omega \in (\omega_2, \omega_4) \text{ for the blue curve,}$$

$$Q[\omega, \omega\tau_{k,1}^+(\omega)] = Q_G(\omega) < 0 \ \text{ for } \omega \in (\omega_3, \omega_1) \text{ for the green curve,}$$

$$Q[\omega, \omega\tau_{k,1}^-(\omega)] = Q_O(\omega) > 0 \text{ for } \omega \in (\omega_3, \omega_1) \text{ for the orange curve}$$

where it should be noticed that $\omega_4 < \omega_3$ under $\alpha < \beta$. According to Theorem 6 given in the Appendix, we now determine the directions of stability switches. The sign of real part of an eigenvalue changes to negative from positive if a pair of (τ_k, τ_h) crosses the blue and green curves in the arrowed directions, and changes to positive from negative through the orange curve. Summarizing the results, we have

Theorem 3 *Assuming a pair of (τ_k, τ_h) moves in the crossing curve in increasing direction of ω, then the stability regions are*

> *1) the left hand side denoted as L_G of the green curve,*
> *2) the right hand side denoted as R_O of the orange curve,*
> *3) the left hand side denoted as L_B of the blue curve.*
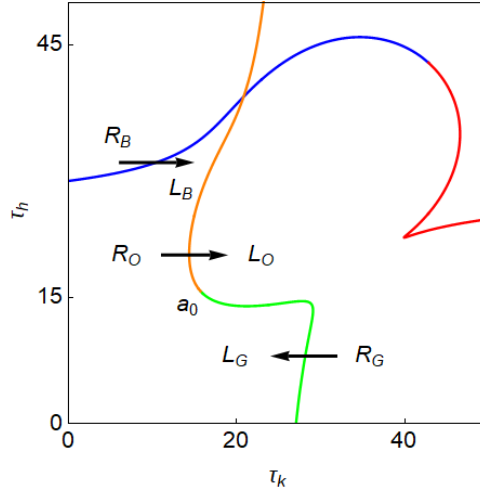
Figure 6 Distorted stability switching curve.

4   Numerical Simulations

We numerically justify the validity of the analytical results obtained in the previous sections. Numerical simulations are done with the symmetric parameter values,

$$\alpha = 1/3, \ \delta = 1/10 \text{ and } s_h = s_k = 1/3.$$

Given constant initial functions,

$$k(t) = k^* + k_0 \text{ and } h(t) = h^* + h_0 \text{ for } t \le 0,$$

we run the delay system (7) for $0 \le t \le T$. Usually data obtained for $t \le 0.9T$ are discarded to take away the effects caused by the initial disturbances. k^* and h^* are the steady state given in (5), k_0 and h_0 are to be determined.[4]

Figure 7 is an enlargement of the lower-right part of Figure 4. It is confirmed that the steady state is locally unstable for (τ_k, τ_h) belonging to the region between the black-red curve and the blue curve, However trajectories (τ_k, τ_h) on the blue curve become sooner or later economically infeasible. The black curve between point c and the point on the abscissa axis is divided into ten small segments. We select one point and fix the value of τ_h at the ordinate of the selected point. We simulate the system (7) with respect to τ_k along the

---

[4]Different values of T, k_0 and h_0 may be chosen in different simulations.

horizontal line at the ordinate. We start from a point whose abscissa is a little bit smaller than the abscissa of the dividing point and increase the value of τ_k until abscissa of the corresponding blue point. The same procedure is repeated along the dotted black curve between c and c'. Similar analysis can be performed on the upper-left part of Figure 4.
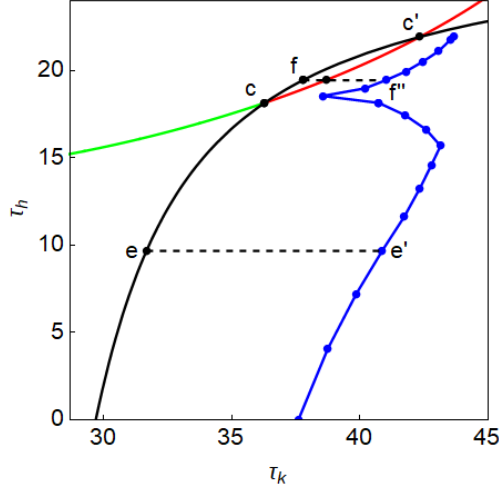
Figure 7 Feasible instability region

In the region between the black curve and the blue curve, the steady state is unstable and cyclic dynamics involving complicated dynamics could arise. Two examples are given in Figure 8. $T = 20,000$, $k_0 = 0.1$ and $h_0 = -0.1$ are common in both simulations.[5] In Figure 8(A), which is essentially the same as Figure 3 of Gori et al. (2016), we select point e with $\tau_k^e \simeq 31.67$ and $\tau_h^e \simeq 9.66$. We repeatedly run the model by increasing τ_k from τ_k^m to τ_k^M (the abscissa of point e') with an increment of $(\tau_k^M - \tau_k^m)/500$ along the lower dotted line in Figure 8 where

$$\tau_k^m = \tau_k^e - 1 \text{ and } \tau_k^M = \tau_k^{e'} = 40.85.$$

It is observed in Figure 8(A) that the steady state is asymptotically stable for $\tau_k \in [\tau_k^m, \tau_k^e)$ since the left hand side of point e is the stability region, loses stability at τ_k^e of point e and then bifurcates to complicated dynamics via period doubling cascade, finally become economically infeasible at $\tau_k^{e'}$ of point e'.

In Figure 8(B), the fixed value of τ_h is increased to $\tau_h^f \simeq 19.43$, the ordinate of point f, and τ_k is increased from τ_k^f to $\tau_k^{f''}$ with an increment of $(\tau_k^{f''} - \tau_k^f)/500$ along the upper dotted line in Figure 6 where

$$\tau_k^f \simeq 37.77 \text{ and } \tau_k^{f''} \simeq 40.99.$$

---

[5]It might be possible to have another critical value of τ_k if we change the value of T. However the change could be only minor and the qualitative property of the blue curve would not be affected.

The steady state is locally unstable for $\tau_k < \tau_k^f$. It is seen in Figure 8(B) that it becomes asymptotically stable for $\tau \in (\tau_k^f, \tau_k^{f'})$ where $\tau_k^{f'} \simeq 38.66$ is the ordinate of point f'' that the crossing point of the dotted line with the red curve of Figure 7. Notice that point f' is seen on the red curve between points c and c' in Figure 5. Although not shown, it is numerically verified that the steady state is locally asymptotically stable for any (τ_k, τ_h) in the lens-shaped region in Figure 5 that proves Theorem 4. The steady state loses stability at $\tau_k^{f'}$ and bifurcates to a limit cycle for larger values of τ_k until $\tau_k^{f''}$ at which economical feasibility is lost. Comparing these two simulations shows that complicated dynamics can be born when the difference between two delays are large and only limit cycle can be observed when the difference is smaller.

(A) With a smaller value of τ_h (B) With a larger value of τ_h
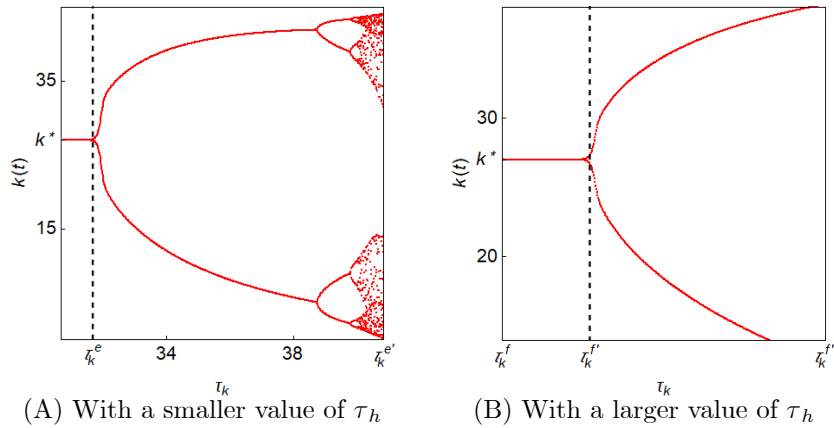
Figure 8. Bifurcation diagrams

5   Concluding Remarks

A delay extended Solow model was developed in which a special Cobb-Douglas production function had three factors, physical capital, human capital and labor. Output was used for investment in physical capital as well as for human capital and consumption. A crucial element of the model was the assumption that construction of the new capitals was delayed due to a gestation time in physical capital and a maturation time in human capital. The stability switching curve on which stability is lost was analytically derived. The theoretical results were numerically confirmed and the study suggests that the delays could be source of endogenous fluctuations. One drawback of the model is that it could not prevent unstable trajectories from being negative maybe due to insufficient nonlinearities of the model.

Appendix

In this Appendix, we provide the stability switching index, Q. When a pair of (τ_k, τ_h) crosses the stability switching curve, we can determine the sign of Q and the direction of the stability loss or gain according to the sign of Q. To this end, we first define a direction of the curve. We call the direction of the curve *positive* if it corresponds to increasing values of ω. When we head in the positive direction of the curve, then the region on our left-hand or right-hand side is called the region on the left (or the L-region) or the region on the right (or the R-region).

Given $P_j(i\omega)$ for $j = 0, 1, 2, 3$, R_ℓ and I_ℓ for $\ell = 1, 2$ denote the real and imaginary parts of

$$P_1(i\omega)e^{-i\omega\tau_k} + P_3(i\omega)e^{-i\omega(\tau_k + \pi_h)} \tag{A-1}$$

and

$$P_2(i\omega)e^{-i\omega\tau_h} + P_3(i\omega)e^{-i\omega(\tau_k + \pi_h)}, \tag{A-2}$$

respectively.

For $\ell = 1$, it is rewritten as

$$i\delta\omega(1-\alpha)\left[\cos(\omega\tau_k) - i\sin(\omega\tau_k)\right] + \delta^2(1-2\alpha)\left[\cos(\omega\tau_k + \omega\tau_h) - i\sin(\omega\tau_k + \omega\tau_h)\right].$$

The real part is

$$R_1 = \delta\omega(1-\alpha)\sin(\omega\tau_k) + \delta^2(1-2\alpha)\cos(\omega\tau_k + \omega\tau_h)$$

that is, with the relations in (16),

$$R_1 = \delta\omega(1-\alpha)\sin(\omega\tau_k) + \delta^2(1-2\alpha)\left[\frac{M}{D}\cos(\omega\tau_k) + \frac{N}{D}\sin(\omega\tau_k)\right]. \tag{A-3}$$

Similarly we can have R_2 if τ_k, τ_h are interchanged,

$$R_2 = \delta\omega(1-\alpha)\sin(\omega\tau_h) + \delta^2(1-2\alpha)\left[\frac{M}{D}\cos(\omega\tau_h) + \frac{N}{D}\sin(\omega\tau_h)\right] \tag{A-4}$$

where $\sin(\omega\tau_h) = -N/D$ and the second part is symmetric in τ_k, τ_h.

The imaginary part of $(A\text{-}1)$ is

$$I_1 = \delta\omega(1-\alpha)\cos(\omega\tau_k) - \delta^2(1-2\alpha)\sin(\omega\tau_k + \omega\tau_h)$$

that can, with the relations in (16), be transformed to

$$I_1 = \delta\omega(1-\alpha)\cos(\omega\tau_k) - \delta^2(1-2\alpha)\left[\frac{M}{D}\sin(\omega\tau_k) - \frac{N}{D}\cos(\omega\tau_k)\right]. \tag{A-5}$$

In the similar way,

$$I_2 = \delta\omega(1-\alpha)\cos(\omega\tau_h) - \delta^2(1-2\alpha)\left[\frac{M}{D}\sin(\omega\tau_h) - \frac{N}{D}\cos(\omega\tau_h)\right] \tag{A-6}$$

where $\cos(\omega\tau_h) = M/D$. Hence the stability switching index is defined as

$$Q(\omega, \omega\tau_k) = R_2 I_1 - R_1 I_2$$

that can be, after arranging the terms, written as

$$
Q(\omega, \omega\tau_k)
$$

$$
= -\frac{N}{D}(\delta\omega)^2(1-\alpha)^2\cos(\omega\tau_k) + \frac{N}{D}B\delta\omega(1-\alpha) + \delta\omega(1-\alpha)A\cos(\omega\tau_k)
$$

$$
-\frac{M}{D}(\delta\omega)^2(1-\alpha)^2\sin(\omega\tau_k) - \frac{M}{D}A\delta\omega(1-\alpha) + \delta\omega(1-\alpha)B\sin(\omega\tau_k)
$$

$$(\text{A-7})$$

where

$$A = \delta^2(1-2\alpha)\left[\frac{M}{D}\cos(\omega\tau_k) + \frac{N}{D}\sin(\omega\tau_k)\right],$$

$$B = \delta^2(1-2\alpha)\left[\frac{M}{D}\sin(\omega\tau_k) - \frac{N}{D}\cos(\omega\tau_k)\right].$$

We have the following result on the direction of any stability switch along the stability switching curves:

Theorem 4 *(Theorem 3 of Matsumoto and Szidarovszky (2018)) Assume $i\omega$ is a simple pure complex eigenvalue and point (τ_k, τ_h) is on the crossing curve. As point (τ_k, τ_h) moves from the right to the left, then a pair of eigenvalues crosses the imaginary axis to the right if $Q(\omega, \omega\tau_k) > 0$ and the direction is opposite if $Q(\omega, \omega\tau_k) < 0$.*

References

Gori, L., Guerrini, L. and Sodini, M., A model of economic growth with physical and human capital: The role of time delays, *Chaos,* 26, 093118, 2016.

Guerrini, L., Matsumoto, A. and Szidarovszky, F., Neoclassical growth model with two fixed delays, *Metroeconomica,* 70*,* 423-441, 2019.

Kalecki, M., A Macroeconomic theory of business cycle, *Econometrica*, 3, 327-344, 1935.

Lin, X. and Wang, E., Stability analysis of delay differential equations with two discrete delays, *Canadian Applied Mathematics Quarterly*, 20, 519-532, 2012.

Mankiw, N., Romer, D. and Weil, D., A contribution to the empirics of economic growth, *Quarterly Journal of Economics*, 107(2), 407-437, 1992.

Matsumoto, A. and Szidarovszky, F., *Dynamic oligopolies with time delays*, Springer-Verlag, Tokyo, 2018.

Solow, R., A contribution to the theory of economic growth, *Quarterly Journal of Economics*, 70, 65-94, 1956.